LWT - Food Science and Technology 187 (2023) 115310

Contents lists available at ScienceDirect

LWT

journal homepage: www.elsevier.com/locate/lwt

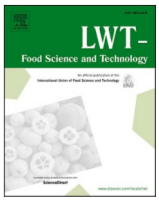

Exploration of efficient SERS features extraction algorithm for rapid detection of thiabendazole residues in apples

Xiaodong Li [a,b], Yanyan Zhang [a,b], Muhammad Awais [a,b], Syed Muhammad Zaigham Abbas Naqvi [a,b], Linze Li [a,b], Hongjun Chen [a,b], Jiandong Hu [a,b,c,*]

[a] College of Mechanical and Electrical Engineering, Henan Agricultural University, Zhengzhou, 450002, China
[b] Henan International Joint Laboratory of Laser Technology in Agricultural Sciences, Zhengzhou, 450002, China
[c] State Key Laboratory of Wheat and Maize Crop Science, Zhengzhou, 450002, China

ARTICLE INFO

Keywords:
Thiabendazole (TBZ)
Surface-enhanced Raman spectroscopy (SERS)
Au@Ag NPs
Nonlinear model
RFE- RF (recursive feature elimination-random forest)

ABSTRACT

Long-term exposure to thiabendazole (TBZ) pesticide residues in fruits can have harmful effects on human health. Therefore, this paper proposes a highly sensitive and time-efficient method for the exploration of efficient SERS feature extraction algorithms to establish an optimal quantitative model for the rapid detection of TBZ residues in apples. Specifically, shape-homogeneous Au@Ag nanoparticles (NPs) were developed as label-free substrates, and the optimal detection time of obtaining SERS signals generated by the binding of TBZ to the substrate sample was determined to be 6 min. Recursive Feature Elimination (RFE) and Competitive Adaptive Reweighted Sampling (CARS) were employed for feature extraction algorithms to optimize characteristic peaks and compare them to full spectra variables and extract effective variables on linear (Ridge, PLS) and nonlinear (SVM, RF) models, respectively. Results showed that the RFE-RF (Recursive Feature Elimination-Random Forest) model was more powerful in variable selection and achieved the highest predictive result of TBZ ($R_P^2 = 0.992$, RMSEP = 0.012 μg/mL) and the computed LOD (Limitation of Detection) was 0.1 μg/mL based on PCA (Principal Component Analysis). Comparison with ELISA verified that the designed method is feasible and potentially applicable to guarantee the safety of pesticide residues in fruits.

1. Introduction

In modern agriculture, pesticides are commonly used to prevent, control, or eliminate pests, diseases, and weeds, which can improve agricultural productivity (Hassan et al., 2021). With the rapid development of agriculture, the use of pesticides has also increased. In 2017, China's pesticide use reached 1.77 million tons, with more than 13 kg of pesticides used per hectare (Meng et al., 2022). Additionally, it is also worth noting that more than half of the applied pesticides have been shown to fall short of the target species and therefore enter environmental elements such as soil, water, and sediment, posing health risks to many environmental organisms, including mankind (Cotton et al., 2016). Strengthening the regulation and control of pesticides and promoting sustainable agriculture, as well as raising awareness and consciousness about pesticides, are therefore important for reducing the negative impacts of pesticides on society.

Thiabendazole (TBZ) is a benzimidazole derivative that can be used as a preservative to prevent and control fungal diseases as well as to maintain the freshness of fruits such as apples (Mueller, David, Chis, & Pinzaru, 2014). When humans consume apples or products containing TBZ residues, the pesticide enters the body through the mouth, stomach, and intestines and is subsequently absorbed into the bloodstream and distributed throughout various tissues and organs. Long-term consumption of apples or apple products containing TBZ residues leads to the accumulation of TBZ in the human body, potentially causing health hazards such as liver, kidney, and nervous system damage (L. Lin, Wu, Liu, Wang, & Yan, 2015). To reduce the risk of human exposure to TBZ, regulatory agencies have established maximum residue limits for TBZ in apples, ensuring that pesticide residues in apples do not negatively impact human health. For instance, the European Union has limited the range of maximum residues of TBZ to 0.05–15 mg/kg in fruits and vegetables (H. Li, Luo, Haruna, Zhou, & Chen, 2023). China has established the highest residue limit for TBZ in apples at 3 mg/kg (GB 2763-2021, 2021).

Over the past few years, various chemical analytical techniques have been developed and applied to detect TBZ concentrations in different

* Corresponding author. College of Mechanical and Electrical Engineering, Henan Agricultural University, Zhengzhou, 450002, China.
E-mail address: jdhu@henau.edu.cn (J. Hu).

https://doi.org/10.1016/j.lwt.2023.115310
Received 20 June 2023; Received in revised form 13 September 2023; Accepted 14 September 2023
Available online 21 September 2023

samples, such as high-performance liquid chromatography (HPLC) (Guilong et al., 2015), liquid chromatography-mass spectrometry (LC-MS) (Zheng et al., 2022), ultra-performance liquid chromatography (UPLC) (Wang, Zang, Zhang, & Wang, 2022), etc. While these techniques offer excellent reproducibility, sensitivity, and accuracy, they also demand significant time, expensive equipment, skilled labor, and intricate pre-processing procedures. Biological methods, such as enzyme-linked immunosorbent assays (Tsialla, Ucles-Moreno, Petrou, Fernandez-Alba, & Kakabakos, 2015), are used for the determination of pesticide residues in samples. The method can provide rapid, reproducible, and economical results but may be affected by interfering factors such as sample complexity, impurities, environmental factors, etc. To overcome these challenges, the development of simple and rapid analytical methods or sensors for TBZ measurement is imminent.

Surface-enhanced Raman spectroscopy is a burgeoning measurement technology that involves the significant enhancement of Raman scattering spectra when the analyte is immobilized on or near a nanostructured surface (Mandal & Tewari, 2022). The mechanism of SERS enhancement can be divided into two components: electromagnetic enhancement and chemical enhancement. The electromagnetic effect is significant when light shines on the nanostructure, generating a local electric field that amplifies the existing electric field. Chemical enhancement arises from the charge transfer between the adsorbed molecule and the nanostructure (Ding, You, Tian, & Moskovits, 2017). In SERS, gold and silver are often used for enhanced detection. Gold nanoparticles are preferred for SERS applications because their preparation is straightforward and their particle morphology is easy to control, making them suitable for label-free detection (Pan et al., 2022). However, silver possesses a stronger plasmon resonance effect than gold, making it more suitable for SERS applications and providing better enhancement (Hussain, Pu, Hu, & Sun, 2021). Nevertheless, silver is more challenging to manipulate into various morphologies than gold (K. Q. Wang, D. W. Sun, H. B. Pu, & Q. Y. Wei, 2019). Thus, Au@Ag bimetallic nanostructures effectively solve this challenge and can provide the desired enhancement. The reserachers (K. Q. Wang, D. W. Sun, H. B. Pu, & Q. Y. Wei, 2019) proposed SERS for rapid determination of difenoconazole in grapes based on Au@Ag nanoparticles aggregates base, with the high performance of detection of 5×10^{-7}–2.5×10^{-5} mol/L difenoconazole in Spiked samples. Chen et al. (Chen et al., 2022) made Au@Ag nanorods of different sizes by adding more AgNO3. They then figured out how to fit three Raman peaks at different concentrations of TBZ in apple or peach juice samples into a single equation. The results that the optical R^2 was 0.99888 and 0.99884 and the LOD in real tests were 0.032 μg/mL and 0.034 μg/mL.

Chemometric models are a range of multivariate analysis techniques that facilitate rapid analysis of detected spectra and allow for a more comprehensive consideration of variables in the spectra, resulting in a more thorough interpretation of the data set and accurate results (J. J. Zhu et al., 2018). When combined with SERS, chemometrics has become a popular research trend for analyzing SERS spectra. Chemometrics involves both pre- and post-processing to construct precise and reasonable quantitative prediction models for food safety indicators. Feature extraction algorithms are included in pre-processing to extract valid information containing the target analytes from the fingerprint spectra of various chemical analytes (A. F. Zhu, Xu, Ali, Ouyang, & Chen, 2021). This approach avoids the selection of only one feature peak from a large amount of analyte feature information to establish the correlation between concentration and Raman intensity, which can result in a reduction in the accuracy and reliability of the established models (Hu et al., 2023; H. H. Li et al., 2022). By utilizing chemometric models, food safety indicators can be accurately and reliably detected, ensuring the safety of food products for consumers. Therefore, it is necessary to introduce chemometric methods in practical spectral analysis applications to better analyze spectral data.

This study investigates the combined utilization of an efficient surface-enhanced Raman scattering (SERS) feature extraction algorithm and a highly sensitive enhanced substrate for the purpose of identifying the optimal quantitative model to rapidly detect thiabendazole in apples. The current study objectives included Au@Ag nanoparticles (NPs) manufacturing as enhanced substrates, followed by the optimal detection time of the SERS signal to obtain SERS spectra of various concentrations of TBZ pesticide residues in apples. Moreover, Competitive Adaptive Reweighted Sampling (CARS) and Recursive Feature Elimination (RFE) were used for feature extraction in the spectral modeling analysis, and the quantitative analysis model was established using linear (Ridge, PLS) and nonlinear (SVM, RF) models. The performance of several models' quantitative prediction accuracy and excellent fit were evaluated using the coefficient of determination (R^2) and root mean square error (RMSE). Finally, the optimal model was validated by recovery analysis with ELISA to meet practical detection needs, which may have practical applications in food quality assessment.

2. Materials and methods

2.1. Materials

Thiabendazole ($C_{10}H_7N_3S$), tetra, silver nitrate ($AgNO_3$), chloroauric acid ($AuCl_3$–HCl–$3H_2O$), anhydrous magnesium sulfate ($MgSO_4$), ascorbic acid (AA), and sodium acetate ($C_2H_3NaO_2$) were collected from Aladdin Reagents Co., Ltd. (Shanghai, China). In contrast, Sigma-Aldrich (USA) purchased sodium citrate ($Na_3C_6H_5O_7$–$2H_2O$) and polyethylene glycol sorbitan monolaurate (Tween20). Acetonitrile (CH_3CN) and methanol (CH_3OH) were purchased from Sinopharm Chemical Reagent Co. This whole research was conducted with analytical-grade reagents that needed no further purification. The apple samples were from a nearby supermarket (Zhengzhou, China). The beakers and magnetic beads used for preparing the precious metal nanoparticles described in this study were soaked in aqua regia overnight and then thoroughly cleaned. All solutions were prepared using ultra-pure water, and necessary analysis was conducted wherever necessary.

2.2. Instruments

This study involved high-quality instrumentation and the analysis of target materials. The UV–Vis spectrometer (Nanjing Filer Instruments Co., Ltd., Nanjing, China) was used to record the UV–Vis spectra of the synthesized Au NPs and Au@Ag NPs within a wavelength range of 300–700 nm. To avoid nanoparticle adsorption on the walls of the tubes, centrifuge tubes were treated with a 0.05% TW20 solution before centrifugation. (Hunan Xiangyi Centrifuge Instrument Co., Ltd.) to scavenge any filth. An oscillator with uniform shaking was used for the solution to synthesize Ag@Au NPs. Images of high-angle annular dark-field scanning transmission electron microscopy (HAADF-STEM) and elemental mapping images taken with an energy-dispersive X-ray spectrometer (EDS) were acquired using the same JEOL JEM-2100 electron microscope. The transmission electron microscopy system from Hitachi, Tokyo, Japan, was used to obtain TEM images of nanoparticles. The confocal Raman microscopy system used to acquire the SERS signal was equipped with a high-stability dark field microscope (BX41, Olympus Co., Center Valley, PA, USA), a confocal Raman module, and a high-resolution spectrometer (Andor Technology LTD, Belfast, BT127AL, USA). Equipped with a German CCD sensor consisting of 1024×256 pixels. The confocal Raman microscopy system was mechanically operated by Beijing Pioneer Technology Ltd., China. To ensure accurate spectra for experimental detection, the samples were pre-calibrated using silicon wafers before testing to guarantee accurate spectra for experimental detection. The laser was focused using a 10 objective with an integration time of 5 s, and Raman spectra in the range of wavelengths from 600 to 1800 cm1 were acquired using the Raman instrument. The instrument parameters were guaranteed to remain unchanged during the experiment.

2.3. Synthesis of Au@Ag NPs

First, the preparation of Au@Ag NPs through seed-mediated growth: Frens's sodium citrate reduction method was used to prepare Au NPs (Frens, G. 1973). Briefly, 950 L of aqueous $HAuCl_4$ solution with a mass fraction of 0.5% was added to a conical flask of 60 mL of ultrapure water. Placed the conical flask on a magnetic stirrer and stirred continuously at 120 °C. After boiling for 2 min, quickly add 500 L of sodium citrate solution with a mass fraction of 1%. When the sodium citrate solution was added, it gradually changed from light yellow to grey-black and finally burgundy. It continued to be heated for 6 min after the color stabilized, then kept cool to room temperature and set aside.

The synthesis of Au@Ag NPs by seed growth method (K. Q. Wang, Sun, Pu, & Wei, 2019a, 2019b)was as follows: 3 mL of Au NPs solution was taken in a centrifuge tube and centrifuged at 8000 rpm for 10 min to get rid of the supernatant, and then the obtained Au NPs were redispersed in 3 mL of ultrapure water. Then a trace amount of 1% sodium citrate solution was added, at last, the sample solution was placed in a centrifuge tube on an oscillator. By controlling the addition of ascorbic acid and silver nitrate, then slowly adding 180 μL of silver nitrate solution with an equal volume of ascorbic acid, maintaining 15 s acceleration per drop, and continuing shaking for 10 min after the color of the solution stabilized, Au@Ag NPs were prepared.

2.4. Preparation and extraction of samples

Concentrate 100 μg/mL of TBZ stock solution was used by adding 1 mg of TBZ pesticide standard to 10 ml of anhydrous methanol. Different concentrations of TBZ solutions (i.e., 0.1, 0.5, 1, 5, 10, and 20 μg/mL) were produced by diluting the stock solution for SERS spectroscopic detection. Fresh juice samples were prepared from existing literature and modified further (Chen et al., 2022). Briefly. juice samples were prepared from fresh apples by coring, grinding, filtering, sterilization, and filtration. Then, 3 mL of TBZ pesticide in various concentrations (0.1, 0.5, 1, 5, 10, 20, and 100 μg/mL) and 1 mL of 1% acetonitrile were mixed with 1 mL of juice. The supernatants were gathered and submitted to further SERS spectrum analysis after being centrifuged at 10, 000 for 8 min with the addition of 0.4 g of $MgSO_4$ and 0.17 g of $C_2H_3NaO_2$.

2.5. SERS measurements and spectral data collection

In each experiment, a single crystal silicon substrate (1 cm × 1 cm) cleaned with acetone, ethanol, and ultrapure water was selected as the solid substrate, and 3 μL of the TBZ standard solution or TBZ juice solution gained was mixed directly with an equal amount of synthesized Au@Ag NPs. From there, 2 μL of the mixture was dripped onto the silicon substrate's surface to form droplets for Raman testing. Since the original SRES spectra usually consist of a pure Raman signal superimposed on the background autofluorescence signal, obtaining the pure Raman signal from the original signal becomes critical. In acquiring the Raman spectral signal, this study uses Vancouver Raman Algorithm software to process the raw Raman spectrum to eliminate the background signal (Zhao, Lui, McLean, & Zeng, 2007).

2.6. Simulation and analysis of the spectra of TBZ computed by density functional theory (DFT)

Gauss 09 software (Gaussian, Inc., Wallingford, CT, USA) was used to compute the theoretical spectra of TBZ. TBZ molecular vibrations were analyzed using B3LYP and 6-31G + (d, p) basis sets.

2.7. Establishing chemometric models

The art of feature extraction and elimination from Raman shift is necessary to optimize feature peaks. The removal of noise from irrelative variables is also necessary to augment the effects posed by real data variables during special feature extraction (J. J. Wang, Chen, Belwal, Lin, & Luo, 2021). The current study was supplemented with CARS and RFE which led to the foundations for the extraction of effects posed by real data variables. Because it can gradually improve feature peaks and remove unfavorable Raman shift variables from the whole SERS spectrum, CARS is a well-liked feature extraction approach. Applying Raman shift variables over the whole SERS spectrum is common practice. The following guidelines apply: Monte Carlo (MC) sampling uses an iterative, competitive process to choose a subset of N variables (H. D. Li, Liang, Xu, & Cao, 2009). The PLS model is examined, and based on the absolute value of the PLS regression coefficients, the weight index of each variable is computed. Then, based on the weighting indicators, critical variables were competitively chosen using the exponentially declining function (EDF) and adaptive reweighted sampling (ARS)(X. Y. Zhu, Li, et al., 2021). The subset was chosen using a 10-fold cross-validation and the root mean square error (RMSE) theory. Finally, variables with small absolute values were removed based on the absolute coefficients calculated from the PLS model in CARS.

Recursive Feature Elimination (RFE) is a powerful variable selection approach that compares weight values supplied during model training (You, Yang, & Ji, 2014). It may be used to minimize feature dimensionality by removing feature redundancy and picking the best mix of features. The prediction model gets trained on the original database, and each variable has a weight assigned to it. Throughout the iterative process, the variables with the lowest absolute weights are removed from the variables set. A combination of a random forest predictor with random variables was used to choose valid and informative variables. The variable selection parameter of 200 was set, and 10% of the features were eliminated in each iteration. Linear (Ridge and PLS) and nonlinear (SVM and RF) algorithms were used to model the quantitative analysis of TBZ in apple samples. To evaluate the predictive capability of the developed calibrated models, the coefficient of determination of the model at calibration (R_C^2) and prediction (R_P^2), RMSEC at calibration, RMSEP at prediction, and RPD were considered. According to previous literature (Dorado, Pinzi, de Haro, Font, & Garcia-Olmo, 2011; X. Wang et al., 2023), the higher the value of good prediction models, the lower the value of RMSE, and usually prediction models greater than 0.9 are worthy of consideration. An RPD is used to judge the predictive power of the model, and a stronger RPD indicates a better predictive ability. In quantitative analysis, the calibration model is considered appropriate if the RPD is greater than 3.

$$R_c^2 = 1 - \frac{\sum_{i=1}^{N}(y_i - \hat{y}_i)^2}{\sum_{i=1}^{N}(y_i - \bar{y}_i)^2} \quad (1)$$

$$R_p^2 = 1 - \frac{\sum_{i=1}^{M}(y_i - \hat{y}_i)^2}{\sum_{i=1}^{M}(y_i - \bar{y}_i)^2} \quad (2)$$

$$RMSEC = \sqrt{\frac{\sum_{i=1}^{N}(y_i - \hat{y}_i)^2}{N}} \quad (3)$$

$$RMSEP = \sqrt{\frac{\sum_{i=1}^{M}(y_i - \hat{y}_i)^2}{M}} \quad (4)$$

$$RPD = \frac{SD}{RMSEP} \quad (5)$$

In the above formula, y_i and $\hat{y}_i$ represent the true and predicted values of the ith sample, respectively; $\bar{y}_i$ represents the average of the true values of all samples; N and M are the number of samples in the correction set and prediction set, respectively; SD is the standard deviation of the true values of all samples in the prediction set.

3. Results and discussions

3.1. Characterization of Au and Au@Ag NPs and the effect of detection time on SERS signals

The Au@Ag NPs are synthesized in a two-step process: first, Au NPs were synthesized using sodium citrate reduction of chloroauric acid, followed by silver nitrate reduction by ascorbic acid. Silver was successively deposited onto the Au NPs surface to produce Au@Ag NPs, whose solution color turned from burgundy to orange (inset of Fig. 1C). The TEM images (Fig. 1A) of the synthesized Au NPs indicated that they are spherical in shape, uniform in morphology, and about 32 nm in diameter. The UV–Vis absorption spectrum of gold nanoparticles exhibited a spectrum peak at 525 nm (Fig. 1C), which was attributed to surface plasmon resonance (SPR) (K. Wang, D.-W. Sun, H. Pu, & Q. Wei, 2019). TEM images (Fig. 1B) showed that the diameter of Au@Ag NPs was about 55 ± 4.5 nm. These Ag@Au NPs were used as enhanced substrates for detecting TBZ pesticide residue. The UV–Vis absorption curves of the synthesized Au@Ag NPs (Fig. 1C) show two distinct peaks at 480 and 409 nm, attributed to the plasmonic properties of gold and silver, respectively. The synthesized Au@Ag NPs were characterized using HAADF-SEM to further validate the Au@Ag structure, and pictures of Au@Ag NPs with an Ag shell (grey filed) and Au core (white filed) are presented in Fig. S1b. As shown in Fig. S1(c-f), the energy spectrum revealed the existence of both Au and Ag components, confirming the successful preparation of Au@Ag NPs. The changes in the SERS signal of TBZ during the evaporation of droplets on silicon wafers were investigated. The SERS spectra of TBZ were collected during all drying procedures of TBZ and AuNPs droplets at 28 °C. During the evaporation of the droplets, Fig. 1D depicts the variation of SERS signals from 1 to 15 min at the SERS peak intensity tested at 775, 896, 1013, 1270, and 1576 cm^{-1}, where the signals increased in the first 6 min and diminished after 7 min. This was attributed to a gradually increasing "coffee ring effect" generated from water evaporation over time, leading to a non-uniform distribution of nanoparticles and samples. (Chen et al., 2022). Hence, All of the experiments below were performed 6 min after the mixed drops were added.

3.2. Detection of TBZ using Au@Ag NPs

The Raman signal enhancement effect of Au@Ag NPs substrate on TBZ molecules was studied. The Raman spectra of 20 μg/mL TBZ bound to Au@Ag NPs and Au NPs with SERS, 100 μg/mL TBZ, and Au@Ag NPs are shown in Fig. S2. The results indicated that the Au@Ag NPs did not affect SERS detection. The SERS of 20 μg/mL TBZ exhibited clear Raman peaks at 775, 896, 1013, 1270, 1576, and 1623 cm^{-1}, whereas the Raman spectrum of 100 ppm TBZ has only a few Raman peaks, with lower Raman intensity than the SERS of TBZ. Previous research has investigated the formation of Ag–S bonds in TBZ molecules on the Au@Ag NPs surface, making TBZ molecules perpendicular to the nanoparticle surface (Oliveira, Rubira, Furini, Batagin-Neto, & Constantino, 2020). According to the surface adsorption selection rule, the SERS signal can be maximally enhanced when the vibrational mode of the absorbed molecule is vertical to the absorbed metal surface (Birke, Znamenskiy, & Lombardi, 2010). To determine the content of TBZ in real food samples, TBZ residue extract of varying concentrations was mixed with Au@Ag NPs substrate at an optimized time for SERS detection. The average spectra for the addition of TBZ (0.1–20 μg/mL) are shown in Fig. 1F. The intensity of the characteristic peak of SERS was found to increase levels of TBZ residues in apple samples.

3.3. Theoretical and experimental Raman spectroscopy analysis of TBZ

Combined software Gauss View 5.0 and Gaussian 09 were applied to compute the theoretical Raman spectroscopy of TBZ molecules and compare it with the experimental SERS at 100 μg/mL. As shown in Fig. 1E, the TBZ SERS spectra, and Raman spectra are nearly identical, and the TBZ Raman peaks are almost identical to the theoretically calculated peaks. Although there are slight shifts at 775, 983, 1013, 1248, 1270, 1457, 1576, and 1623 cm^{-1} at 18 cm^{-1}, this has no bearing on the designation of the feature peaks. However, Remarkably, the Raman signature peak at the SERS signature peak of 896 cm^{-1} was detectable, while 1412 cm^{-1} was only calculated theoretically. This may be because the theoretical calculation only considered the vibration mode of the molecule in the ideal state and did not take into account the effect of TBZ molecule-solvent interaction (J. J. Zhu et al., 2018). There

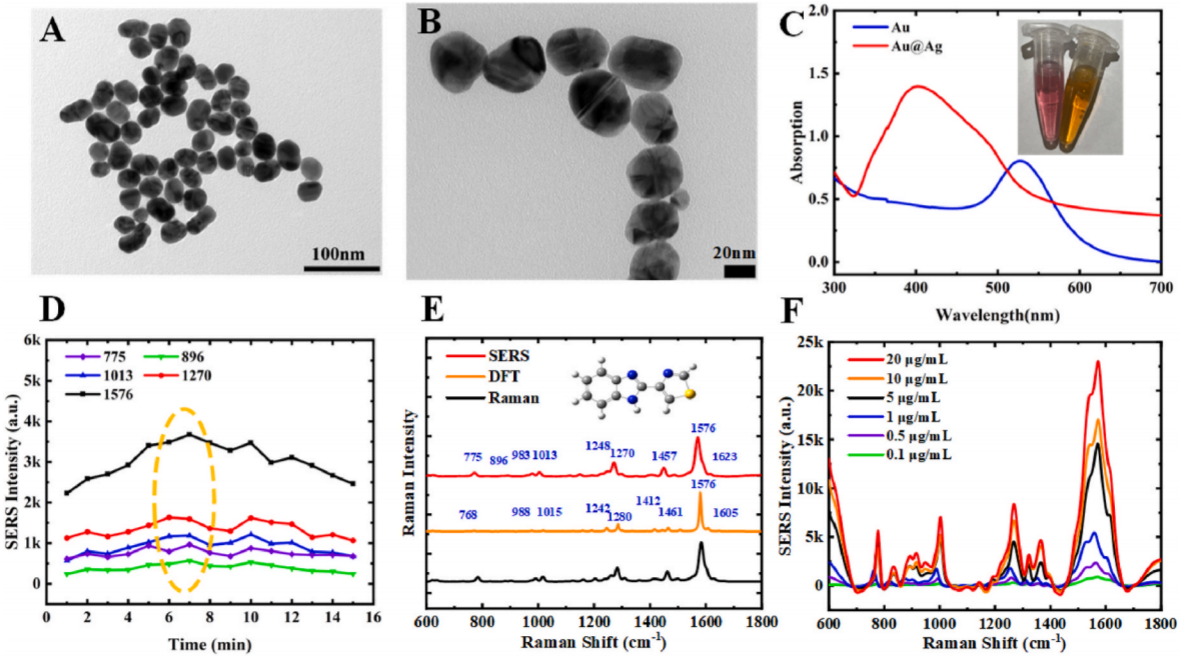

Fig. 1. The TEM image (A), TEM image (B), UV–Vis absorption spectra (C) of Au NPs and Au@Ag NPs, SERS signals of TBZ with different times of Au NPs (D). The theoretical and experimental Raman spectra of TBZ (E) and the average spectra of TBZ residues with different concentrations (F).

are various functional groups (Fig. 1E inset) that make up the TBZ molecule, such as -C-H-, –C═H-, -C-C-, and -N-H-, etc. Each chemical bond corresponds to a specific spectral feature peak. The main features are identified in Table S1. The characteristic peaks are part of C–S stretching vibration and C═N bending vibration at 775 cm^{-1}, and C–S tensile vibration at 983 cm^{-1}. At 1013 and 1270 cm^{-1} belong to C–N tensile vibrations and C–H bending vibrations, at 1457, 1576, and 1623 cm^{-1} belong to C═N tensile vibrations, and at 1248 cm^{-1} there are both C–N and C═C tensile vibrations and C–H bending vibrations.

3.4. Results of chemometric model prediction

3.4.1. Results of ridge, PLS, SVM, and RF models

This study explored the implications of redundant information in the SERS spectral acquisition process on analytical results. To improve the spectral signal-to-noise ratio, background information was subtracted from the original spectra using the Vancouver Raman Algorithm. The full spectra were analyzed for different TBZ concentrations using quantitative modeling techniques including Ridge, PLS SVM, and RF. 84 spectra were selected as the trained collection and 29 as the prediction collection to evaluate the predictability and generalization ability of the developed models. Table 1 provides the result of the proposed model in detail. It can be seen that the R_C^2 of Ridge and RF is a maximum of 0.999, while the R_P^2 of Ridge is a minimum of 0.871 and the RPD is 2.882 does not satisfy the requirements. The R_P^2 and RPD for the RF model are the largest and the RMSEP is the smallest. SVM and PLS were comparable in effectiveness, close to 0.98 and both greater than 0.96, but the RPD values of SVM were greater than PLS, indicating better predictive performance. Overall, the RF model performs better in quantifying TBZ and has the best prediction potential. Compared to the linear model, the nonlinear model has a higher RPD and a lower RMSEP value. These models were ranked based on the above metrics: RF > SVM > PLS > Ridge.

3.4.2. CARS-ridge, CARS-PLS, CARS-SVM, and CARS-RF models results

Although the Vancouver Raman algorithm software is employed to prevent background signal interference, there is an implausibility between the prediction results of the detection model, which may be due to the influence of the model by the spectral peak overlap and redundant extraneous information. To enhance the accuracy and reliability of the results, using feature extraction to mitigate these effects is an effective way. Further development of quantitative models explored the likelihood of CARS and RFE algorithms independently to acquire valid Raman shift variables and to eliminate TBZ-independent information in the original SERS spectra. The CARS method was executed several times in this study to optimize the results in Fig. 2. The number of MC sampling runs was set to 50. Fig. 2A illustrates how the parameters such as the number of samples, RMSECV, and regression coefficients of variables of each wave number vary. In **Fig. 2A(a)**, it gradually reduced the number of sampled variables through two stages of fast selection and fine selection, and the best variables subset was achieved according to the minimum RMSECV principle in Fig. 2A(b). The regression coefficient paths for each variable are documented in Fig. 2A(c). When the number of samples is 22, the ideal variable subset with the minimum RMSECV is indicated by the vertical line of the blue dashed line. The Ridge, PLS, SVM, and RF regression models using 54 variables for TBZ are shown in Fig. 2 (B, C, E, and F). The results of the models are all satisfactory, demonstrating that CARS improves the reliability of the models. Notably, the CARS-PLS and CARS-Ridge models improved slightly with R_P^2 = 0.944 and 0.972, respectively, with a decrease in RMESE. Compared with the CARS-RF model, CARS-SVM had a slightly worse predictive performance. CARS-RF was the effective prediction model with R_C^2 = 0.999, RMSEC = 0.076 μg/mL, R_P^2 = 0.984, RMSEP = 0.015 μg/mL, and RPD = 7.986.

3.4.3. RFE-ridge, RFE-PLS, RFE-SVM, and RFE-RF model results

The number of variables selected in each RFE iteration steadily decreases until the necessary features are selected. By aiming for the optimal prediction, the required number of features is optimized to end up at 160. As shown in Fig. 2 (G and J), after the selection of variables by RFE selection, the ranking of the optimal variables obtained for 160 variables is shown in red, and the points in red represent variables from the optimal collection of variables observed in the spectrum. The spectral variables in the RFE selection correspond to the strong peak near TBZ, as well as the weak peak nearby. As can be seen in Table 1 and Fig. 2 (H, I, K, and L), the RFE-RF achieved significantly higher R_P^2 and RPD values than CARS and full spectrum based on the RFE-selected variables, and the RMSEP value decreased to 0.012 μg/mL. However, RFE-Ridge, RFE-PLS, and RFE-SVM did not see a significant improvement, likely due to the random forest's feature selection mechanism, which can automatically detect the important features in the dataset to improve prediction ability. Therefore, RFE-RF was considered a practical model with R_C^2 = 0.999, RMSEC = 0.067 μg/mL, R_P^2 = 0.992, RMSEP = 0.012 μg/mL, and RPD = 11.352.

3.4.4. Discussion and analysis of chemometric models

For establishing the optimization quantification model of TBZ, regression models based on full-spectrum data were first developed using Ridge, PLS, SVM, and RF. However, the models' performance could still be improved due to the large RMSE and low R_P^2 values produced by the models. Therefore, a variable selection approach was implemented to reduce redundant variables and utilize information on variables to enhance model performance and stability. With the CARS model, 64 feature variables from the full spectrum were selected, and as seen in Table 1, the R_P^2 and RPD values of CARS-Ridge, CARS-PLS, and CARS-SVM models were improved. The CARS-RF model performs the

Table 1
Statistical results of four quantification algorithms based on full spectra (PLS, Ridge, RF, and SVM) combined with the variables selection approaches (CARS and RFE) for thiabendazole.

Variable selection	Algorithm type	Algorithms	Calibration set		Prediction set		RPD
			R_C^2	RMSEC (μg/mL)	R_P^2	RMSEP (μg/mL)	
Origin	Linear	Ridge	0.999	0.004	0.871	0.263	2.882
		PLS	0.983	0.093	0.964	0.153	4.943
	Nonlinear	SVM	0.979	0.106	0.963	0.146	5.211
		RF	0.999	0.088	0.986	0.022	8.564
CARS	Linear	Ridge	0.998	0.031	0.944	0.190	3.984
		PLS	0.993	0.030	0.972	0.131	5.772
	Nonlinear	SVM	0.989	0.095	0.972	0.132	5.732
		RF	0.999	0.076	0.984	0.015	7.986
RFE	Linear	Ridge	0.979	0.104	0.942	0.177	4.284
		PLS	0.977	0.208	0.935	0.208	3.657
	Nonlinear	SVM	0.984	0.090	0.967	0.137	5.522
		RF	**0.999**	**0.067**	**0.992**	**0.012**	**11.352**

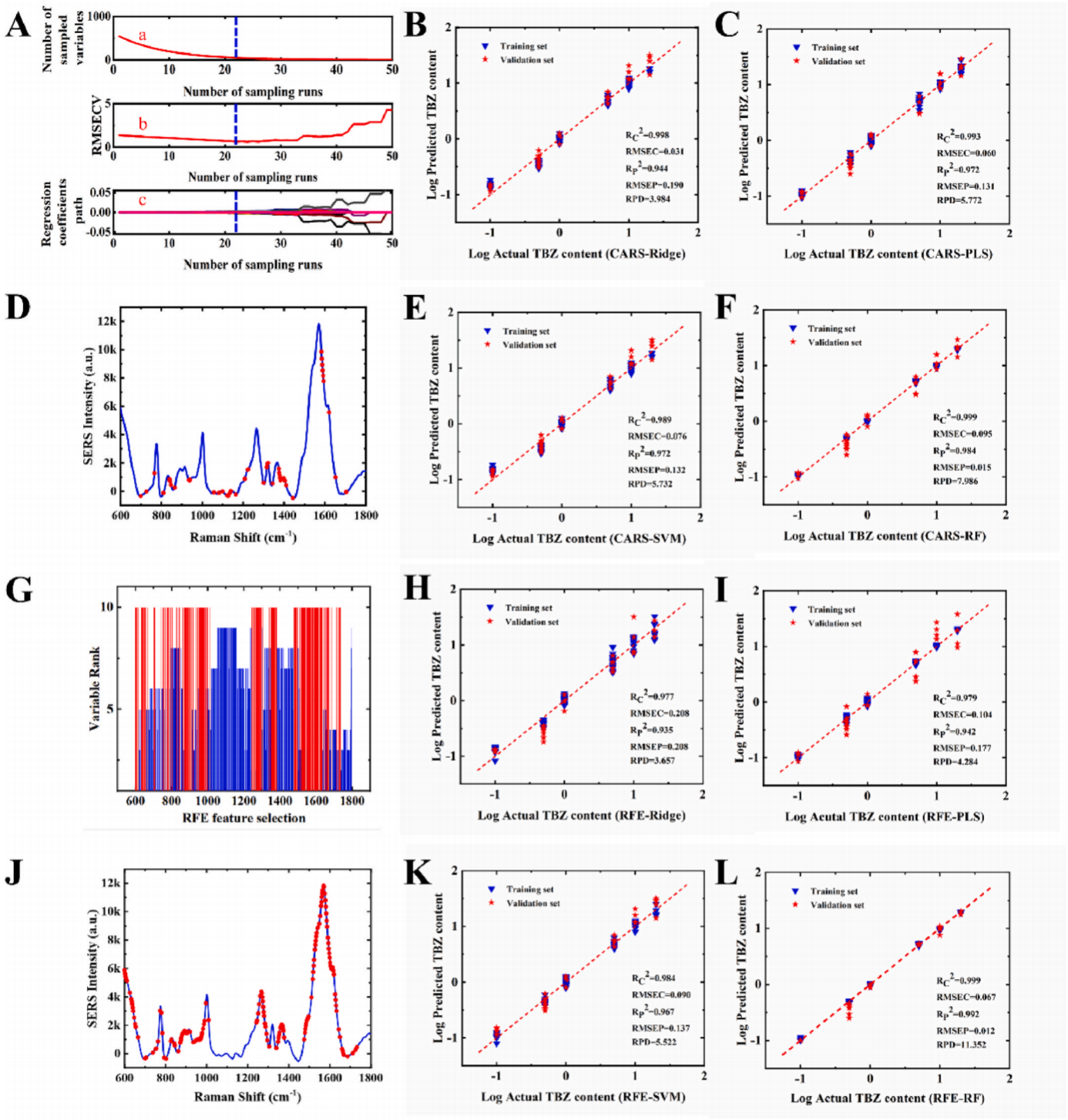

Fig. 2. The results of feature extraction and model prediction. The variables selection process of CARS (A), The best variable selection of CARS (D), Scatter plots of the true and predicted values of TBZ for the training and test sets obtained using CARS-Ridge (B), CARS-PLS (C), CARS-SVM (E) and CARS-RF (F). The variables ranking of RFE (G), The best variable selection of RFE (J), Scatter plots of the true and predicted values of TBZ for the training and test sets obtained using RFE -Ridge (H), RFE -PLS (I), RFE -SVM (K) and RFE –RF (L).

best, but the results are not as good as the full-spectrum combined RF model, because the features acquired using CARS are the result of selecting the best after many runs, such that the information of all valid features cannot be extracted stably. Optimizing the RFE by selecting the number of feature sets as 160, the results show that only the RFE-RF model has improved performance compared to CARS, which demonstrates that RFE extracts more effective feature information than CARS. Noticeably, RF has high prediction performance and stability regardless of whether it is combined with the feature extraction algorithm. Therefore, the RFE-RF model was considered for application in TBZ detection.

The RFE-RF model provided the highest robustness, efficiency, and accuracy in predicting TBZ concentrations with $R_P^2 = 0.992$ and RPD = 11.352. As seen from the results in Table 1, regardless of which variable selection method is used, the nonlinear regression model (SVM, RF) outperforms the linear regression model (PLS, Ridge). The results of the

linear model differ significantly before and after the application of the feature extraction model, while the nonlinear algorithm obtains a stable improvement with all R_P^2 values greater than 0.96. Nonlinear algorithms have stronger fitting and generalization abilities compared to linear algorithms and are trained to learn and model the correlation with Raman intensity and concentration, resulting in less inaccuracy and more precise models.

3.5. Stability, reproducibility, and specificity of Au@Ag NPs SERS sensors

The Au@Ag NP's stability and reproducibility were evaluated by the continuous collection of SERS spectra of TBZ. In Fig. 3, the average spectra from samples of the same concentration over 8 days show good agreement, with the Au@Ag NPs staying well dispersed and homogeneous with no agglomeration. The RSD of SERS intensity at 1576 cm^{-1} was 8.29%, further demonstrating the reproducibility of Au@Ag NPs. Anti-interference experiments were performed to investigate the effect of other pesticide residues in common fruit juices, such as dimethoate, chlorpyrifos, thiram, and trichlorfon. As shown in Table S2, the developed method could successfully identify the signature bands of TBZ independently of additional added pesticides, in case of overmixing of TBZ with additional pesticides. With no TBZ, the developed method detected only trace amounts of TBZ with different signature bands and intensities of additional residues. Those results confirmed the promising specificity and selectivity of the designed sensor for TBZ detection.

3.6. Recovery analysis and limit of detection (LOD)

To assess the predictive performance of the SERS combined RFE-RF model, TBZ sample recovery analysis was performed. For recovery analysis, several samples were recovered for analysis The prepared juice sample solutions with TBZ concentrations (10, 5, 0.5 μg/mL) were sampled separately and mixed with Au@Ag NPs were detected on clean silicon wafers. For each concentration, a complete of 6 spectra were collected. The acquired SERS spectra were imported into the optimal RFE-SVM model for contaminant prediction, and subsequently, calculations were made for recoveries of three different concentrations in the samples. Additionally, the present method was demonstrated by the ELISA with the predicted values and recoveries of the samples from both SERS and ELISA shown in Table 2. The recoveries were 99%–106% for SERS and 102%–103% for ELISA. For both methods, the relative standard deviations (RSD) were below 5%, meeting the requirements for pesticide residue analysis, and there were no obvious differences between the SERS and the ELISA. Considering that the LOD (limit of detection) is a crucial parameter of the proposed newly designed methods, it is no exception for SERS sensors. In the case of SERS sensors, the LOD was determined by the minimum detectable concentration of the method. PCA (principal component analysis) is a linear dimensionality reduction method, where the original sample points in a high-dimensional space are linearly projected into a low-dimensional space by some projection matrix to achieve dimensionality reduction (S. Lin et al., 2023). The minimum detection concentration was computed by PCA analysis, which involves analyzing a diverse set of data with different concentrations (minimum) including blanks (H. H. Li et al., 2022). Fig. 4 shows the different clusters for different concentrations. The first three PCs of TBZ contributed. According to the principal component analysis, the first three PCs accumulated to retain the relevant information of the objective analytes. Thus, the proposed TBZ sensor was chosen for the LOD of 0.1 μg/mL, following the limitation level by the Chinese Ministry of Agriculture for apple juice. The sensor was contrasted with other reported methods for TBZ detection, as shown in Table 3 (Birke et al., 2010; Boeris, Arancibia, & Olivieri, 2014; Damm et al., 2011; Feng, Hu, Grant, & Lu, 2018; He, Chen, & Labuza, 2014; H. Li et al., 2023; Liou, Nayigiziki, Kong, Mustapha, & Lin, 2017; Raveendran & Docoslis, 2021; Yu et al., 2023). Although conventional methods such as ELISA and LC-MS require longer sample pretreatment and complex extraction methods, have low LODs, and outperform SERS, this method has fast and simple pretreatment and short detection time and possesses lower detection limits than other SERS. Accordingly, the Au@Ag NPs-based SERS sensor used in this study can reliably detect TBZ in complex situations due to its stability and simplicity.

4. Conclusions

This work aimed to explore efficient SERS feature extraction algorithms for rapid detection of thiabendazole residues in apples. Ag@Au NPs with uniform shape and excellent enhancement effects were synthesized by a two-step method to acquire SERS spectra of TBZ. To reduce the impact of the "coffee ring" effect, the optimal SERS detection time was chosen to be 6 min for the drip-drying process. The CARS and RFE algorithms were used to obtain effective features from the full spectrum to improve the efficiency of the model operation as well as the prediction accuracy. Linear (Ridge and PLS) and nonlinear (SVM and RF) algorithms combining full spectrum and effective features were employed to build quantitative models. The results indicated that the combined RFE-RF model as an optimal quantitative model was more capable of selecting features and exhibited the best prediction performance for TBZ ($R_P^2 = 0.992$, RMSEP = 0.012 μg/mL). The LOD was deemed to be 0.1 μg/mL according to the PCA. Furthermore, the developed approach exhibited excellent sensitivity with recovery ranging between 99 and 106% and RSD of not more than 5%, and the results were not significantly different from those obtained by ELISA, demonstrating the high feasibility and accuracy of Ag@AuNPs-based SERS coupled with RFE-RF

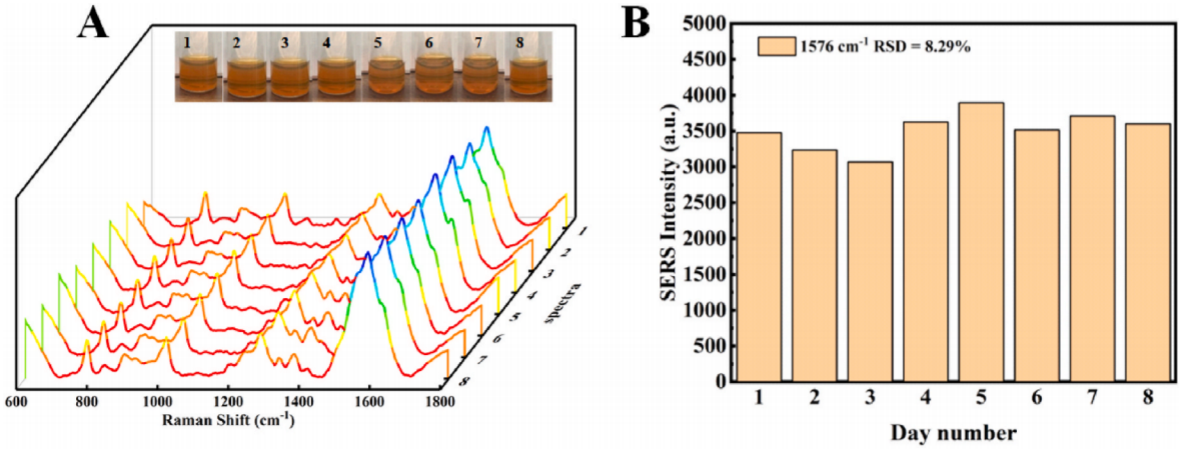

Fig. 3. Stability and reproducibility testing: Average SERS spectra of TBZ and Au@Ag NPs for eight consecutive days (A), Spectral intensities at 1576 cm^{-1} (B).

Table 2
The result from the developed method and ELISA for TBZ detection in spiked samples.

Spiked concentration (μg/mL	The developed method			ELISA		
	Prediction value (μg/mL) (Mean[a] ± SD[b])	RSD (%)	Recovery (%)	Detection value (μg/mL) (Mean[a] ± SD[b])	RSD (%)	Recovery (%)
10	10.07 ± 0.49	4.95	99	10.22 ± 0.13	1.31	102
5	5.38 ± 0.23	4.34	106	5.19 ± 0.21	2.12	103
0.5	0.49 ± 0.01	3.0	99	0.52 ± 0.21	2.06	103

[a] Mean: the average value of six tests.
[b] SD: standard deviation, n = 6.

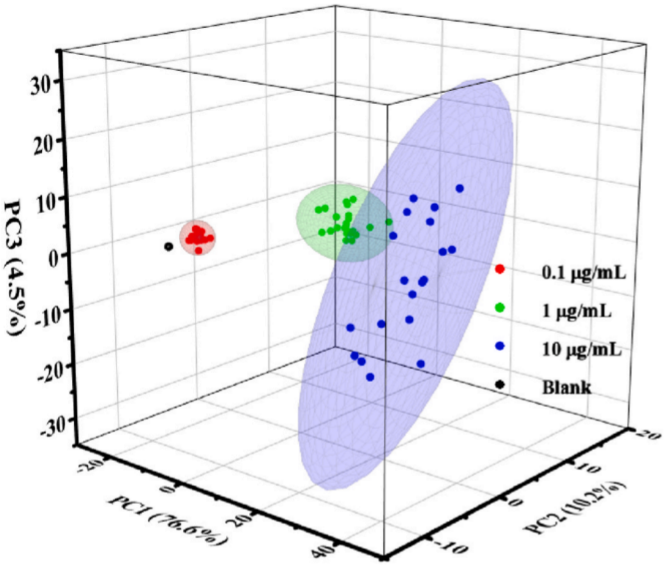

Fig. 4. Three-dimensional principal component analysis for thiabendazole with different concentrations (Blank, 0.1 μg/mL, 1 μg/mL, and 10 μg/mL). Principal component PC1 represents 76.6% variance, PC2 represents 10.2% variance and PC3 represents 4.5% variance.

Table 3
Comparison of R^2 and LODs of several methods for thiabendazole.

Method	Tested sample	Data analysis	R^2	LOD (μg/mL)	References
HPLC	Apple juice	Linear regression	0.999	1.5	Birke et al. (2010)
SERS	Apple	PLS	0.977	0.1	He et al. (2014)
SERS	Apple juice	Logarithmic fitting	0.988	0.1	Yu et al. (2023)
SERS	Fruit juice	PLS	0.975	0.14	(Damm et al., 2011)
SERS	Mango juice	Logarithmic fitting	0.99	0.179	Boeris et al. (2014)
SERS	Apple, pear, orange	Regression fitting	0.98	0.24	Li et al. (2023)
SERS	Apple, Water	Linear regression	0.97	1	Raveendran and Docoslis (2021)
MISPE-SERS	Orange juice	Multivariate analysis	0.9371	4	Feng et al. (2018)
SERS	Apple			5	Liou et al. (2017)
SERS	Apple juice	Regression fitting	**0.992**	**0.1**	**This work**

for rapid prediction of TBZ in apple samples. Overall, the SERS in combination with advanced chemometric techniques, is believed to have the potential for rapid and quantitative detection of TBZ residues in fruits, which can contribute to effective monitoring of food safety. Nevertheless, the SERS substrates synthesized by the chemical method in this paper have certain defects that need further research and innovation, while the study of deep learning for quantitative analysis of Raman signals is gradually increasing, and it is also worthwhile for researchers to explore this research.

CRediT authorship contribution statement

Xiaodong Li: Conceptualization, Methodology, Investigation, Writing – original draft. **Yanyan Zhang:** Methodology, Investigation. **Muhammad Awais:** Software, Formal analysis, Methodology. **Syed Muhammad Zaigham Abbas Naqvi:** Methodology, Investigation. **Linze Li:** Writing – review & editing, Formal analysis, Funding acquisition. **Hongjun Chen:** Software. **Jiandong Hu:** Supervision, Project administration, Resources, Funding acquisition, All authors have read and agreed to the published version of the manuscript.

Declaration of competing interest

The authors declare that they have no known competing financial interests or personal relationships that could have appeared to influence the work reported in this paper.

Data availability

Data will be made available on request.

Acknowledgments

The authors are thankful to the National Natural Science Foundation of China (grant number 32071890, 31671581) and the Henan Provincial Science and Technology Research Project (GZS2021007).

Appendix A. Supplementary data

Supplementary data to this article can be found online at https://doi.org/10.1016/j.lwt.2023.115310.

References

Birke, R. L., Znamenskiy, V., & Lombardi, J. R. (2010). A charge-transfer surface enhanced Raman scattering model from time-dependent density functional theory calculations on a Ag 10-pyridine complex. *The Journal of Chemical Physics, 132*(21), Article 214707. https://doi.org/10.1063/1.3431210

Boeris, V., Arancibia, J. A., & Olivieri, A. C. (2014). Determination of five pesticides in juice, fruit and vegetable samples by means of liquid chromatography combined with multivariate curve resolution. *Analytica Chimica Acta, 814*, 23–30. https://doi.org/10.1016/j.aca.2014.01.034

Chen, Z. Y., Sun, Y., Shi, J. Y., Zhang, W., Zhang, X. A., Huang, X. W., et al. (2022). Facile synthesis of Au@Ag core-shell nanorod with bimetallic synergistic effect for SERS detection of thiabendazole in fruit juice. *Food Chemistry, 370*, 131276. https://doi.org/10.1016/j.foodchem.2021.131276

Cotton, J., Leroux, F., Broudin, S., Poirel, M., Corman, B., Junot, C., et al. (2016). Development and validation of a multiresidue method for the analysis of more than 500 pesticides and drugs in water based on on-line and liquid chromatography coupled to high resolution mass spectrometry. *Water Research, 104*, 20–27. https://doi.org/10.1016/j.watres.2016.07.075

Damm, C., Segets, D., Yang, G., Vieweg, B. F., Spiecker, E., & Peukert, W. (2011). Shape transformation mechanism of silver nanorods in aqueous solution. *Small, 7*(1), 147–156. https://doi.org/10.1002/smll.201001600

Ding, S.-Y., You, E.-M., Tian, Z.-Q., & Moskovits, M. (2017). Electromagnetic theories of surface-enhanced Raman spectroscopy. *Chemical Society Reviews, 46*(13), 4042–4076. https://doi.org/10.1039/C7CS00238F

Dorado, M. P., Pinzi, S., de Haro, A., Font, R., & Garcia-Olmo, J. (2011). Visible and NIR Spectroscopy to assess biodiesel quality: Determination of alcohol and glycerol traces. *Fuel, 90*(6), 2321–2325. https://doi.org/10.1016/j.fuel.2011.02.015

Feng, J., Hu, Y., Grant, E., & Lu, X. (2018). Determination of thiabendazole in orange juice using an MISPE-SERS chemosensor. *Food Chemistry, 239*, 816–822. https://doi.org/10.1016/j.foodchem.2017.07.014

Frens, G. (1973). Controlled nucleation for the regulation of the particle size in monodisperse gold suspensions. *Nature; Physical Science, 241*(105), 20–22.

G B 2763-2021 G. (2021). *National food safety standard – maximum residue limits for pesticides in food*.

Guilong, P., Qiang, H., Daniel, M., Guangming, Z., Weiliang, P., Li, G., et al. (2015). Vortex-assisted liquid-liquid microextraction using a low-toxicity solvent for the determination of five organophosphorus pesticides in water samples by high-performance liquid chromatography. *Journal of Separation Science, 38*(20), 3487–3493. https://doi.org/10.1002/jssc.201500547

Hassan, M. M., Jiao, T. H., Ahmad, W., Yi, X., Zareef, M., Ali, S., et al. (2021). Cellulose paper-based SERS sensor for sensitive detection of 2,4-D residue levels in tea coupled uninformative variable elimination-partial least squares. *Spectrochimica Acta Part A: Molecular and Biomolecular Spectroscopy, 248*, Article 119198. https://doi.org/10.1016/j.saa.2020.119198

He, L., Chen, T., & Labuza, T. P. (2014). Recovery and quantitative detection of thiabendazole on apples using a surface swab capture method followed by surface-enhanced Raman spectroscopy. *Food Chemistry, 148*, 42–46. https://doi.org/10.1016/j.foodchem.2013.10.023

Hu, Y., Ma, B., Wang, H., Zhang, Y., Li, Y., & Yu, G. (2023). Detecting different pesticide residues on Hami melon surface using hyperspectral imaging combined with 1D-CNN and information fusion. *Frontiers of Plant Science, 14*, Article 1105601. https://doi.org/10.3389/fpls.2023.1105601

Hussain, A., Pu, H. B., Hu, B. X., & Sun, D. W. (2021). Au@Ag-TGANPs based SERS for facile screening of thiabendazole and ferbam in liquid milk. *Spectrochimica Acta Part A: Molecular and Biomolecular Spectroscopy, 245*, Article 118908. https://doi.org/10.1016/j.saa.2020.118908

Li, H. H., Hassan, M. M., He, Z. F., Haruna, S. A., Chen, Q. S., & Ding, Z. (2022). A sensitive silver nanoflower-based SERS sensor coupled novel chemometric models for simultaneous detection of chlorpyrifos and carbendazim in food. *LWT-Food Science & Technology, 167*, 113804. https://doi.org/10.1016/j.lwt.2022.113804

Li, H. D., Liang, Y. Z., Xu, Q. S., & Cao, D. S. (2009). Key wavelengths screening using competitive adaptive reweighted sampling method for multivariate calibration. *Analytica Chimica Acta, 648*(1), 77–84. https://doi.org/10.1016/j.aca.2009.06.046

Li, H., Luo, X., Haruna, S. A., Zhou, W., & Chen, Q. (2023). Rapid detection of thiabendazole in food using SERS coupled with flower-like AgNPs and PSL-based variable selection algorithms. *Journal of Food Composition and Analysis, 115*, 105016. https://doi.org/10.1016/j.jfca.2022.105016

Lin, S., Fang, X., Fang, G., Liu, F., Dong, H., Zhao, H., et al. (2023). Ultrasensitive detection and distinction of pollutants based on SERS assisted by machine learning algorithms. *Sensors and Actuators B: Chemical, 384*, 133651. https://doi.org/10.1016/j.snb.2023.133651

Lin, L., Wu, R.-m., Liu, M.-h., Wang, X.-b., & Yan, L.-y. (2015). Surface-enhanced Raman spectroscopy analysis of thiabendazole pesticide. *Spectroscopy and Spectral Analysis, 35*(2), 404–408. https://doi.org/10.3964/j.issn.1000-0593(2015)02-0404-05

Liou, P., Nayigiziki, F. X., Kong, F. B., Mustapha, A., & Lin, M. S. (2017). Cellulose nanofibers coated with silver nanoparticles as a SERS platform for detection of pesticides in apples. *Carbohydrate Polymers, 157*, 643–650. https://doi.org/10.1016/j.carbpol.2016.10.031

Mandal, P., & Tewari, B. S. (2022). Progress in surface enhanced Raman scattering molecular sensing: A review. *Surfaces and Interfaces, 28*, 101655. https://doi.org/10.1016/j.surfin.2021.101655

Meng, Z., Cui, J., Li, R., Sun, W., Bao, X., Wang, J., et al. (2022). Systematic evaluation of chiral pesticides at the enantiomeric level: A new strategy for the development of highly effective and less harmful pesticides. *Science of the Total Environment, 846*, 157294. https://doi.org/10.1016/j.scitotenv.2022.157294

Mueller, C., David, L., Chis, V., & Pinzaru, S. C. (2014). Detection of thiabendazole applied on citrus fruits and bananas using surface enhanced Raman scattering. *Food Chemistry, 145*, 814–820. https://doi.org/10.1016/j.foodchem.2013.08.136

Oliveira, M. J. S., Rubira, R. J. G., Furini, L. N., Batagin-Neto, A., & Constantino, C. J. L. (2020). Detection of thiabendazole fungicide/parasiticide by SERS: Quantitative analysis and adsorption mechanism. *Applied Surface Science, 517*, 145786. https://doi.org/10.1016/j.apsusc.2020.145786

Pan, H., Ahmad, W., Jiao, T., Zhu, A., Ouyang, Q., & Chen, Q. (2022). Label-free Au NRs-based SERS coupled with chemometrics for rapid quantitative detection of thiabendazole residues in citrus. *Food Chemistry, 375*, Article 131681. https://doi.org/10.1016/j.foodchem.2021.131681

Raveendran, J., & Docoslis, A. (2021). Detection and quantification of toxicants in food and water using Ag-Au core-shell fractal SERS nanostructures and multivariate analysis. *Talanta, 231*, 122383. https://doi.org/10.1016/j.talanta.2021.122383

Tsialla, Z., Ucles-Moreno, A., Petrou, P., Fernandez-Alba, A. R., & Kakabakos, S. E. (2015). Development of an indirect enzyme immunoassay for the determination of thiabendazole in white and red wines. *International Journal of Environmental Analytical Chemistry, 95*(13), 1299–1309. https://doi.org/10.1080/03067319.2015.1100727

Wang, J. J., Chen, Q. S., Belwal, T., Lin, X. Y., & Luo, Z. S. (2021). Insights into chemometric algorithms for quality attributes and hazards detection in foodstuffs using Raman/surface enhanced Raman spectroscopy. *Comprehensive Reviews in Food Science and Food Safety, 20*(3), 2476–2507. https://doi.org/10.1111/1541-4337.12741

Wang, S. H., Zang, X. H., Zhang, S. H., & Wang, J. P. (2022). Determination of benzimidazoles in beef by molecularly imprinted boron nitride composite based dispersive solid phase microextraction and ultra performance liquid chromatography. *Microchemical Journal, 179*, 107523. https://doi.org/10.1016/j.microc.2022.107523

Wang, X., He, L., Xu, L., Liu, Z., Xiong, Y., Zhou, W., et al. (2023). Intelligent analysis of carbendazim in agricultural products based on a ZSHPC/MWCNT/SPE portable nanosensor combined with machine learning methods. *Analytical Methods, 15*(5), 562–571. https://doi.org/10.1039/d2ay01779b

Wang, K., Sun, D.-W., Pu, H., & Wei, Q. (2019a). Surface-enhanced Raman scattering of core-shell Au@Ag nanoparticles aggregates for rapid detection of difenoconazole in grapes. *Talanta, 191*, 449–456. https://doi.org/10.1016/j.talanta.2018.08.005

Wang, K. Q., Sun, D. W., Pu, H. B., & Wei, Q. Y. (2019b). Shell thickness-dependent Au@Ag nanoparticles aggregates for high-performance SERS applications. *Talanta, 195*, 506–515. https://doi.org/10.1016/j.talanta.2018.11.057

Wang, K. Q., Sun, D. W., Pu, H. B., & Wei, Q. Y. (2019c). Surface-enhanced Raman scattering of core-shell Au@Ag nanoparticles aggregates for rapid detection of difenoconazole in grapes. *Talanta, 191*, 449–456. https://doi.org/10.1016/j.talanta.2018.08.005

You, W. J., Yang, Z. J., & Ji, G. L. (2014). Feature selection for high-dimensional multi-category data using PLS-based local recursive feature elimination. *Expert Systems with Applications, 41*(4), 1463–1475. https://doi.org/10.1016/j.eswa.2013.08.043

Yu, X., Sun, Y., Hu, J., Wang, J., Zhuang, X., Zhang, S., et al. (2023). MoS2/Au/Ag nanostructures for ratiometric surface-enhanced Raman scattering determination of pesticide residues. *ACS Applied Nano Materials, 6*(1), 685–694. https://doi.org/10.1021/acsanm.2c04843

Zhao, J., Lui, H., McLean, D. I., & Zeng, H. (2007). Automated autofluorescence background subtraction algorithm for biomedical Raman spectroscopy. *Applied Spectroscopy, 61*(11), 1225–1232. https://doi.org/10.1366/000370207782597003

Zheng, D., Hu, X., Fu, X., Xia, Z., Zhou, Y., Peng, L., et al. (2022). Flowerlike Ni-NiO composite as magnetic solid-phase extraction sorbent for analysis of carbendazim and thiabendazole in edible vegetable oils by liquid chromatography-mass spectrometry. *Food Chemistry, 374*, Article 131761. https://doi.org/10.1016/j.foodchem.2021.131761

Zhu, J. J., Agyekum, A. A., Kutsanedzie, F. Y. H., Li, H. H., Chen, Q. S., Ouyang, Q., et al. (2018). Qualitative and quantitative analysis of chlorpyrifos residues in tea by surface-enhanced Raman spectroscopy (SERS) combined with chemometric models. *LWT-Food Science & Technology, 97*, 760–769. https://doi.org/10.1016/j.lwt.2018.07.055

Zhu, X. Y., Li, W. J., Wu, R. M., Liu, P., Hu, X., Xu, L. L., et al. (2021). Rapid detection of chlorpyrifos pesticide residue in tea using surface-enhanced Raman spectroscopy combined with chemometrics. *Spectrochimica Acta Part A: Molecular and Biomolecular Spectroscopy, 250*, 119366. https://doi.org/10.1016/j.saa.2020.119366

Zhu, A. F., Xu, Y., Ali, S., Ouyang, Q., & Chen, Q. S. (2021). Au@Ag nanoflowers based SERS coupled chemometric algorithms for determination of organochlorine pesticides in milk. *LWT-Food Science & Technology, 150*, 111978. https://doi.org/10.1016/j.lwt.2021.111978